BILINGUAL PUBLISHING GROUP

Journal of Architectural Environment & Structural Engineering Research

https://journals.bilpubgroup.com/index.php/jaeser

ARTICLE

Resilience of an Observation Wheel in Bangkok: Reflections on March 28, 2025, the Mw 7.7 Mandalay Earthquake

Samard Buddee

FSE Consultant Co., Ltd., Bangkok 10210, Thailand

ABSTRACT

On March 28, 2025, the Mw 7.7 earthquake (EQ) in Mandalay, Myanmar caused the largest amount of damage from a local or regional EQ in modern Thai history. It spread to the capital city of Bangkok, Thailand, an epicentral distance of 1,000 km, where tall buildings swayed and were damaged; most notably, a 33-storey office building collapsed in response. This study aims to determine the safety of an existing observation wheel, located in Bangkok, for resisting EQs in terms of displacements and storey drift ratios of the steel structure, including the stability of existing reinforced concrete foundations. It was built in 2012, when the seismic loads for Bangkok appeared to be very small. Thus, wind "out of service" loadings of 100 mph were considered the dominant lateral force, leading to structures designed primarily for wind. A safety evaluation applied loads by using the original wind loading and updated spectral accelerations including seven selected ground motions for Mw 7.62 EQs from NGA-West2. As a result, the max displacements of the wind and EQ loads were under the IBC 2021 deflection limit, the max storey drift ratios of the EQ loads were under the ATC 40 and DPT 1301/1302-61 storey drift ratio limits, and the shaking effects from the EQ on the foundations were less than the forces from the wind, which governed the foundation design of the existing structure. Consequently, the observation wheel has adequate resilience for resisting seismic loads from EQs, as shown by the March 28, 2025 Mw 7.7 Mandalay EQ.

Keywords: Resilience; Observation Wheel; Earthquake; Steel Structure; Foundation; Wind

*CORRESPONDING AUTHOR:

Samard Buddee, FSE Consultant Co., Ltd., Bangkok 10210, Thailand; Email: samard@fseworld.org

ARTICLE INFO

Received:4 June 2025 | Revised: 10 July 2025 | Accepted: 18 July 2025 | Published Online: 26 July 2025

DOI: https://doi.org/10.30564/jaeser.v8i3.13125

CITATION

Buddee, S., 2025. Resilience of an Observation Wheel in Bangkok: Reflections on March 28, 2025, the Mw 7.7 Mandalay Earthquake. Journal of Architectural Environment & Structural Engineering Research. 8(3): 26–46. DOI: https://doi.org/10.30564/jaeser.v8i3.13125

1. Introduction

On March 28, 2025, the M_W 7.7 Mandalay EQ occurred along the Sagaing fault at a depth of 10.0 km along Mandalay down to Nay Pyi Taw in the north-central Myanmar province of Mandalay, causing the largest amount of damage from a local or regional EQ in modern Thai history [1]. This was also the first time in the modern history of continental Southeast Asia that an EQ with a magnitude greater than 7.5 was caused by one of the major active faults. It spread to the capital city of Bangkok (BKK), an epicentral distance of 1,000 km (**Figure 1**), where tall buildings swayed and were damaged in response. Despite damage to buildings and infrastructure in BKK, there was only one collapse: a 33-story building under construction, which resulted in 109 casualties [2].

BKK was built on deep and soft alluvial soil (**Figure 2**), which can amplify incoming ground motion even from events occurring hundreds of kilometers away. BKK has geological conditions very well aligned to yield destruction from distant subduction EQs, as seen during the EQ. The surficial geologic setting, and the ability of regional sources, caused this to become a major EQ in BKK.

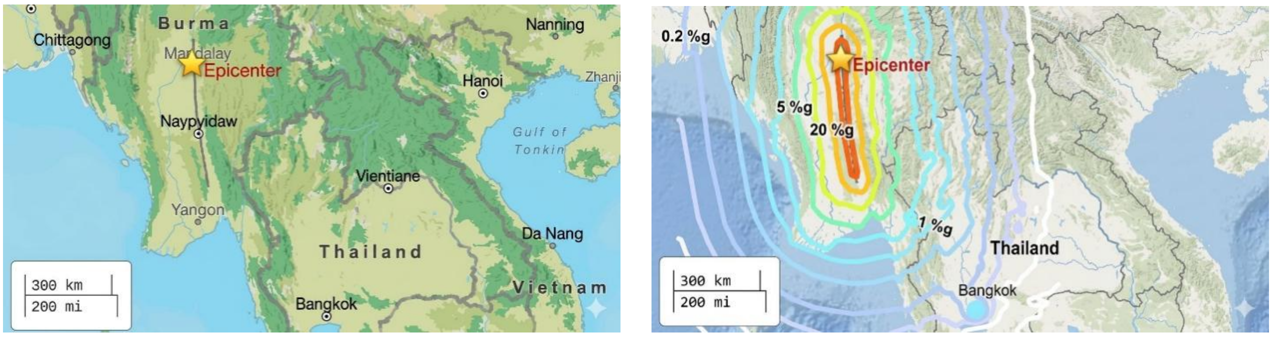

(**a**) (**b**)

Figure 1. (**a**) Epicenter and Finite Fault of the Mw 7.7 EQ, Mandalay, 2025, and (**b**) PGA contours.

Source: USGS.

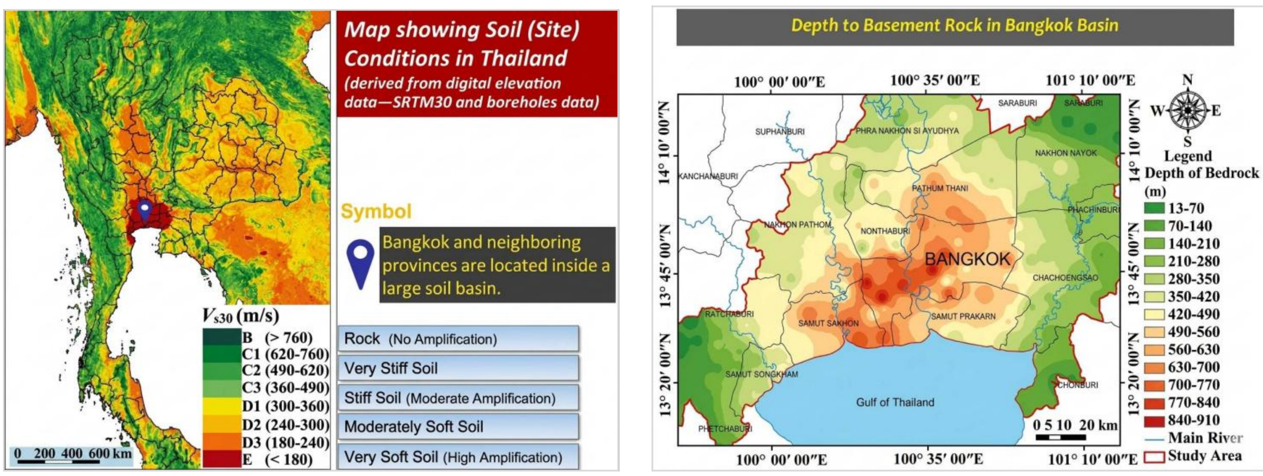

(**a**) (**b**)

Figure 2. (**a**) Soil conditions in Thailand: BKK and neighboring provinces are located inside a large soil basin (dark red, site class "E", V_{s30} < 180 m/s), and (**b**) depth of bedrock in the BKK basin.

Source: Dr. Pennung Warnitchai, Asian Institute of Technology.

Figure 3 shows the 10-zone seismic microzonation map of BKK (Zone 5) and surrounding provinces, and seismic design spectrums for 10 zones (damping = 5% for reinforced concrete buildings). In strong wind terrain, when traditional design codes are employed, the wind demands can be higher than the seismic design demands, and therefore, can control the design. However, studies have shown that the level of design wind load can alter the seismic performance of high-rise dual system buildings [3], and the wind-governed design can alter the seismic performance of high-rise buildings [4,5]. Bending moment due to Wind force is increased in a steel structure for a high-rise building. However, the bending moment due to Seismic force is reduced in a steel structure for a high-rise building [6].

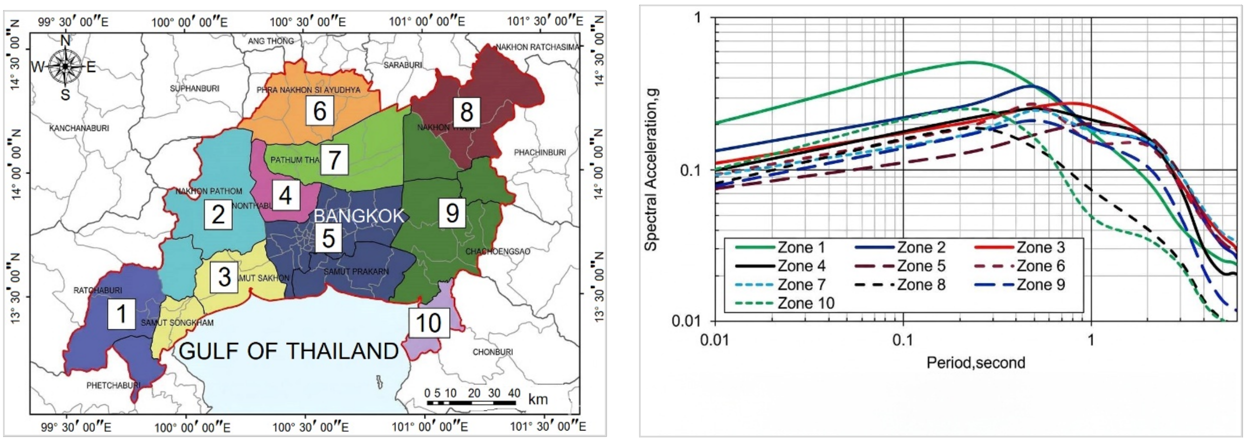

(**a**) (**b**)

Figure 3. (**a**) The 10 zones DPT1301/1302-18 seismic microzonation map and (**b**) the new design spectra (Damping = 5.0%) for Bangkok (Zone 5) and surrounding provinces.

2. Problem Statement

The old design spectral accelerations (Sa) (DPT1302-9 standard) [7,8] were established based on the data of the site characteristics available in the past.

After several moderate earthquakes in northern Thailand, including the 2011 Mw 6.8 Tarlay earthquake and the 2014 Mw 6.1 Mae Lao earthquake [9], new design spectral accelerations for BKK were developed in 2017 [10]. The DPT1301/1302-18 seismic design regulation [11,12] was issued in 2018 with several updates, including seismic hazard assessments.

The existing structure [13] for this case study is located in BKK, Thailand. It was designed and built in 2012, when the old seismic loads for BKK appeared to be very small as mentioned above. Thus, wind “out of service” loadings of 100 mph were considered the dominant lateral force, leading to structures designed primarily for wind.

For this case study, the shaking effects from the Mw 7.7 Mandalay earthquake on foundations may have been smaller than the forces from the wind loading, so that the wind loading may govern the foundation design of this existing steel structure.

Consequently, there is a need to evaluate the resilience of the existing structure.

3. Objective of the Study

This study aims to evaluate the resilience of the existing structure for resisting the seismic loads of an EQ, in particular the 28 March 2025 Mw 7.7 Mandalay EQ, by comparing max storey displacements (DPMs) from different load inputs with the IBC 2021 DPM limit; comparing max interstorey drift ratios (IDRs) from different load inputs with the DPT1301/1302-18 and ATC 40 standard IDR limits; comparing forces at the base of the leg columns from different load inputs with loads from original wind loading to check the stability of existing footings; and comparing max axial forces of applicable selected main member loads from the different load inputs with the wind load.

4. Methodology

Figure 4 shows the scheme of the case study methodology. Linear modeling will be applied to the case study buildings, using ELF, RSA, and WL, and also nonlinear modeling will be applied by using NLRHA to check the accuracy, the global responses and compare all of the procedures.

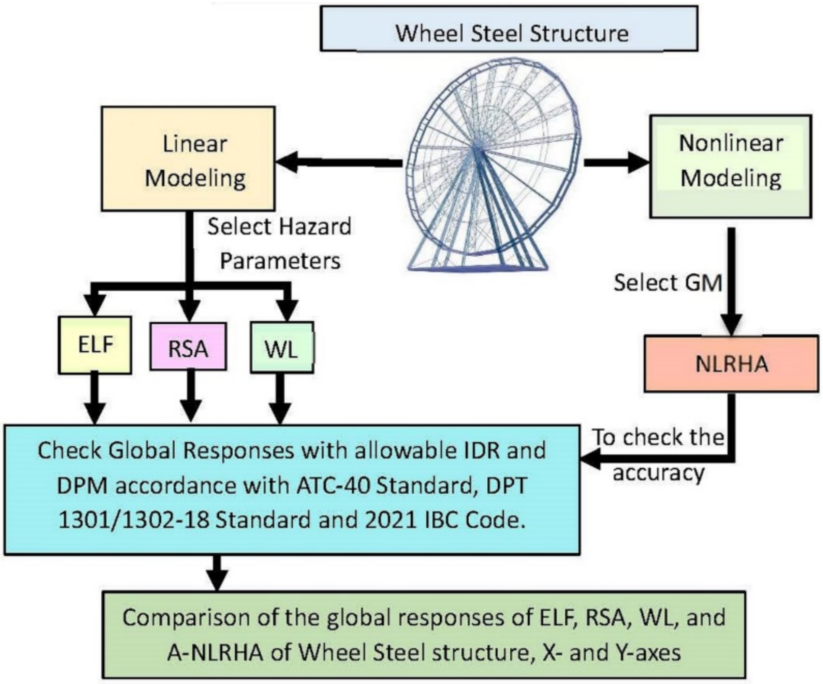

Figure 4. The scheme of the case study methodology.

5. Details of the Existing Structure

The structure is located by the Chao Phraya, which is the major river in Thailand (**Figure 5**). The ground floor level of the observation wheel is an average elevation of only about 1.5 m above mean sea level. It was designed as a medium observation wheel measuring a diameter (∅) of 50.5 m; a height (H) of 28 m for the main axle, and 53.25 m to the top of a wheel; a base width of 24.62 m; and a base depth of 19.61 m. There are 42 gondolas and 21 spokes.

The entire observation wheel is a special steel structure, supported by a central tower and a radial structure, and all loads transfer down to the 8-steel legs, which are established on its own reinforced concrete (RC) foundation with 6-bored piles. The bored piles have a diameter of ∅ 350 mm and a depth of 20 m. The bored piles, in essence, are then only required to resist vertical uplifts and downwards reactions arising from EQ loads, wind loads, and floods. Therefore, connections are required between the pile and pile caps in accordance with ACI 318-99 code: 25.4 [14,15].

Figure 5. The existing observation wheel.

Material Specifications

(1) Concrete strength, f'c
The f'c is 28 MPa for general structures.

(2) Reinforcement bar strength
The yield strength of the bar diameters of 6–9 mm and 12–28 mm is 240 MPa and 400 MPa, respectively, as per ASTM A615 standard [16].

(3) Steel strength
The yield and tensile strengths of steel are 350 and 450 MPa, respectively, as per ASTM A500 [17], ASTM A501 [18], ASTM A572 [19] and DPT 1304-61 standards [20].

(4) Steel wire rope strength
The steel wire rope with tensile strength of 1,180 MPa is adopted as the standard cable and diagonal tie elements, as per BS EN 12385 standard [21].

(5) Member types and sections
Member types and sections are shown in **Table 1**.

Table 1. Types and sections of members (steel).

No.	Names	Type	Size (mm)	Thickness (mm)
1	Support Leg	Column	∅ 762.0	12.70
2	Main axle	Beam	∅ 457.0	45.0
			∅ 141.3	15.88
3	Spoke	2-D truss	∅ 76.3	4.00
			∅ 48.3	5.08
4	Circular tie	Bracing	∅ 64.0	3.20
5	Diagonal cable	Bracing	∅ 20.0	-
6	Circular rim	Beam	SHS 320 × 320	15.00

6. Evaluation of the Resilience

6.1. Modelling

Figure 6 shows 3-dimensional (D) models for the front elevation and the side elevation of the existing observation wheel steel structure. Based on simulation studies of similar observation wheels, the wheel steel structural system is typically modeled using finite element methods (FEM) for stiffness. The steel structure is often modeled using structural dynamics to determine modal frequencies and to simulate the interaction between moving masses and the fixed structure. A cable bracing system is a lightweight but strong solution that provides lateral stability for steel structures. Using high-strength steel cables, it helps steel structures resist wind and earthquakes while keeping construction cost-efficient and flexible. Gondolas are treated as concentrated masses (point masses) that move along the structural elements. In complex simulations, the gondola can be a separate node in a multi-element model (e.g., separating the car from the attachment points) to study pitch and roll dynamics.

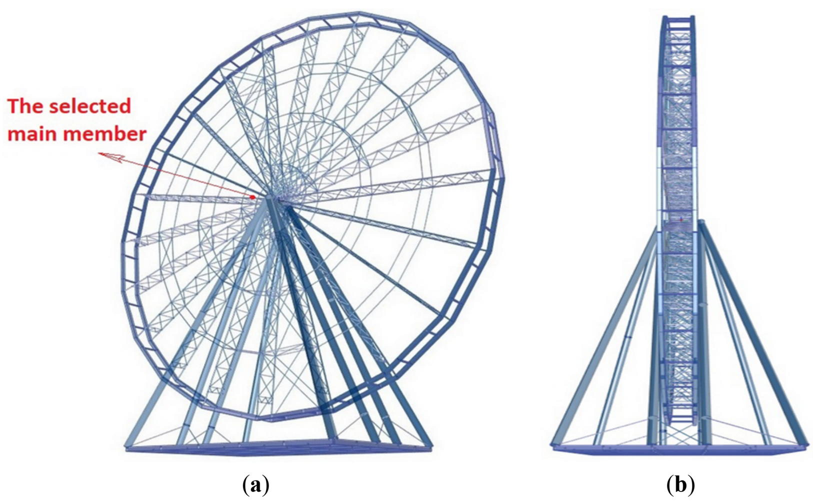

Figure 6. 3-dimensional models: (**a**) Front elevation, one (red) of the main members is selected for comparing the maximum axial loads from the different load inputs with the wind load. It has a diameter of 141.3 mm with a thickness of 15.88 mm as shown in item No. 3 of **Table 1**, and (**b**) Side elevation.

6.2. Load Analysis

6.2.1. Static Loadings

Dead loads (DLs) of concrete, steel, water, and soil densities are 24 kN/m^3, 78.5 kN/m^3, 10 kN/m^3, and 18 kN/m^3, respectively, and the weight of a gondola is 4.3 kN. Live loads (LLs) are movable loads and skipped with a skip factor of 0.75. The LL of the ticketing area is 5 kN/m^2 and the LL (8 persons) per gondola is 6 kN. The superimposed dead load (SDL) of a concrete topping is 1.2 kN/m^2.

6.2.2. Seismic Loadings

For wind load, an original wind speed design (in 2012), "wind out of service", is 100 mph (1,140 N/m²), which is higher than the wind speed standard for Bangkok (85 mph or 25 m/s) as shown in **Figure 7** [22]. Exposure type is C (**Figure 8**) [23], topographical factor (*Kzt*) is 1, gust factor (*Gf*) is 2.35 (DPT 1311-07 standard; item B.3 in pages 75–80, for open or special structures) [24], directionality factor (*Kd*) is 0.85, important factor (*I*) is 1.0, and solid/gross area ratio is 0.2.

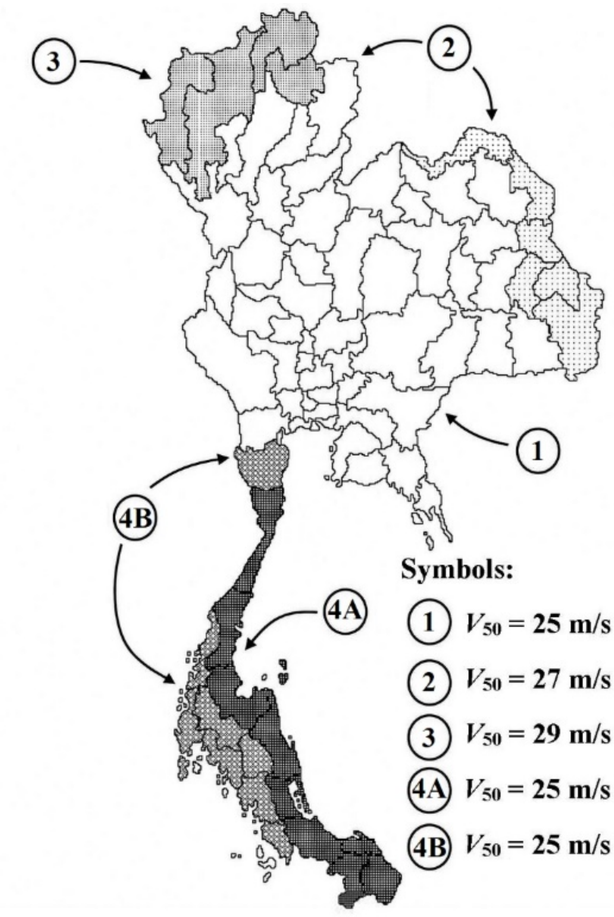

Figure 7. Reference wind speed zone in Thailand.

Figure 8. The existing structure is located by the Chao Phraya River.

For wind design, the observation wheel structure qualifies as an open structure. **Figure 9** shows a seismicity map of Thailand and surrounding areas (M > 5, during 1922–2023) by Thailand's Earthquake Observation Division (EOD) under the Thai Meteorological Department (TMD). **Figure 10** shows the DPT1301/1302-18 seismic design spectrum for zone 5 for Damping = 2.5% and Damping = 5.0%.

Designs to resist wind loads and seismic loads are similar only in the fact that load effects are represented by horizontal forces acting at the story levels. In fact, part of the appeal of the equivalent static lateral force method is that the application of external loads and the computation of member forces for design is the same as it is for wind loading. The ASCE 7-05 standard does not suggest an allowable drift limit for wind design as it does for seismic design. The 2021 IBC code (Table 1604.3a) [25] suggests that for secondary wall members supporting formed metal siding, the design wind load deflection shall not exceed l/90. Seismic drift is recognized as inelastic drift because of the inelastic behavior of the seismic force-resisting system. Thus, a deflection amplification factor, Cd, is used to account for an inelastic drift. On the other hand, wind drift is considered an elastic drift because the wind force-resisting system interacts linearly with the design wind forces. **Table 2** shows the parameters of Zone 5 (damping = 2.5%, the dashed blue lines in **Figure 10**). BKK is classified under Zone 5 (**Figure 3a**). **Table 3** shows the modal participating mass ratios and the summary of the first three modes on the x- and y-axes.

Due to the real-time ground motion data from the 2025 Mw 7.7 Mandalay EQ (recorded by TMD), which were not available at the time of the analysis. **Figure 11** shows the ground acceleration (PGA) map from the magnitude 8.2 earthquake in Myanmar on March 28, 2025, at 13:20 local time, recorded by EOD under TMD. The earthquake, centered 326 km northwest of Pang Mapha, Mae Hong Son, caused significant shaking across Thailand, with peak acceleration up to 0.2 g at Bhumibol Dam. The selection of 7-Mw 7.62 records simulates the 2025 Mw 7.7 Mandalay EQ, which caused long-period ground shaking in BKK. These similar, high-energy, and long-period records were used to accurately represent the seismic hazards from this major event to BKK's soft soil, as shown in studies of far-field motion characteristics. **Table 4** shows the seven selected ground motion (SGM) parameters, which are selected from thirty-four ground motions from PEER: Time Series Search Report-NGA-West2-2025-09-29 [26]; Magnitude Min–Max = 7.4–8.1, Rrup Min–Max = 30–200 km, Rjb Min–Max = 30–200 km, V_{s30} Min–Max = 660–860 m/s, D9-95 Min–Max = 10–60 s. **Figure 12** shows accelerations of the 7 SGMs compared to the real-time acceleration of the Mw 7.7 Mandalay EQ in the north and east directions. For BKK clay, V_{s30} is less than 180 m/s. Modification of parameters: the DPT 1301/1302-61 standard, particularly the updated versions, recognizes the specific site effects of the BKK Basin. Modified parameters (such as S_1, S_s, F_a, F_v) from the standard's tables are required for this case study to accurately reflect the amplification. This modified approach accurately accounts for the dramatic change in soil properties between the source (V_{s30} = 760 m/s) and the site (V_{s30} < 180 m/s) according to the DPT 1301/1302-61 standard as shown in **Figure 10** and **Table 2**.

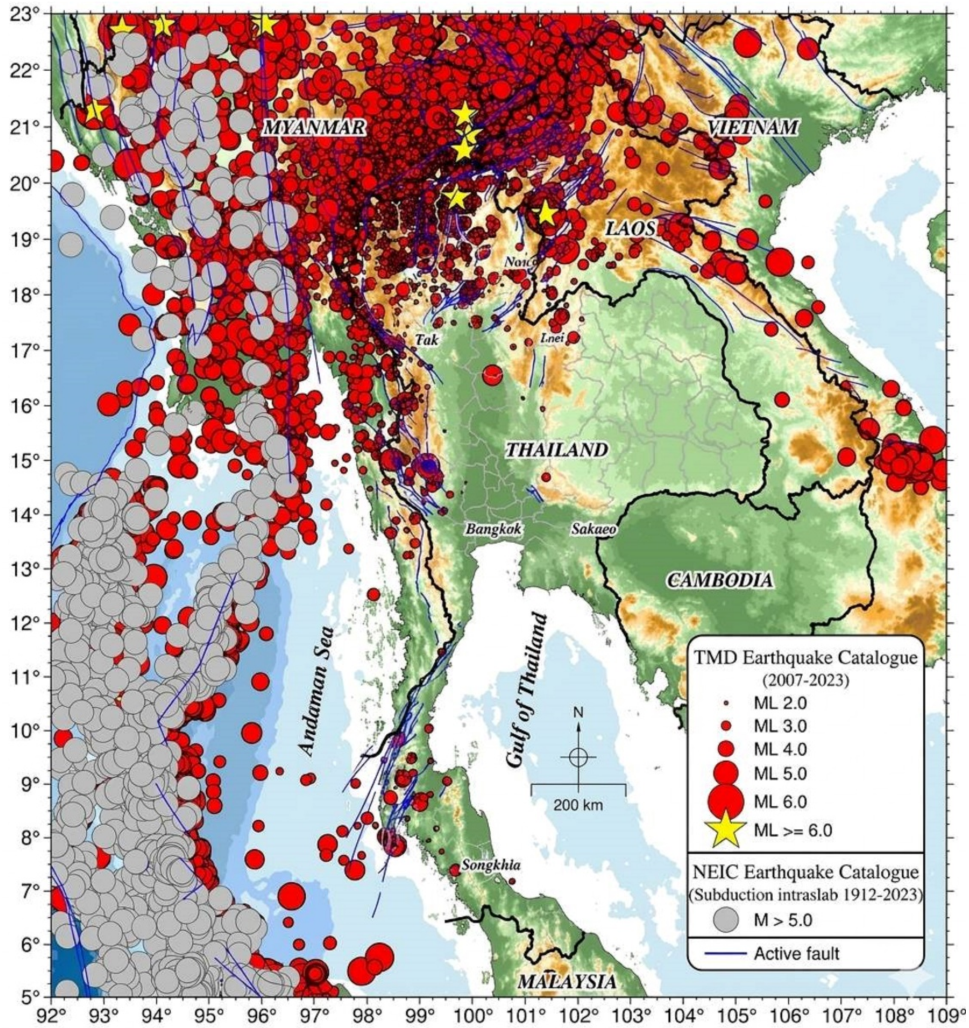

Figure 9. Probabilistic Seismicity hazard map of Thailand and surrounding areas used in seismic hazard analysis, which comprises earthquake catalogue obtained from the USGS-NEIC (M > 5, during 1922–2023) of subduction earthquake (gray) and TMD earthquake catalogue between 2007–2023 (red).

Source: Patinya Pornsopin, the Earthquake Observation Division (EOD) under the Thai Meteorological Department (TMD).

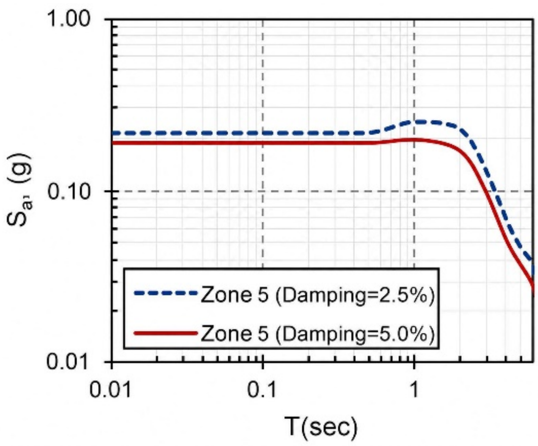

(**a**)

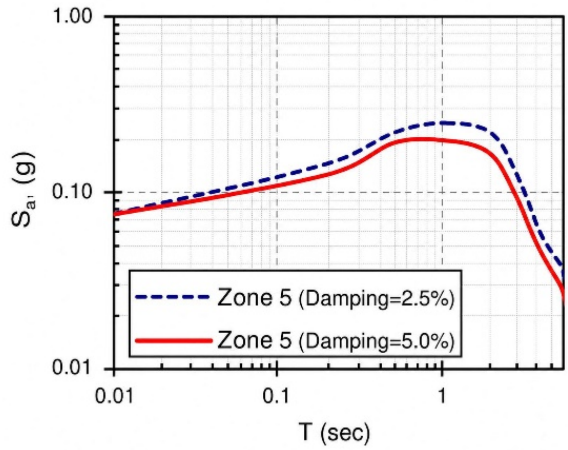

(**b**)

Figure 10. The DPT1301/1302-18 seismic design spectrum for Zone 5 in case of damping = 2.5%, and 5.0%: (**a**) The equivalent static lateral force, and (**b**) the response spectrum.

Table 2. Parameters of Zone 5.

Parameter	Value
Response modification factor, R	3.500
Occupancy importance factor, I	1.250
Damping ratio, ξ	0.025
System overstrength factor, Ω_o	3.000
Deflection amplification factor, C_d	3.000
Long-period transition period, s	6.00
Site class	E
MCE, 2% in 50 years at 0.2 s, SDS dynamic, g	0.148
MCE, 2% in 50 years at 1.0 s, SD1 dynamic, g	0.250
MCE, 2% in 50 years at 0.2 s, SDS static, g	0.191
MCE, 2% in 50 years at 1.0 s, SD1 static, g	0.250
Maximum number of modes	140

Note: damping = 2.5%, the dashed blue lines in **Figure 10**.

Table 3. Modal participating mass ratios and summary of the first three modes.

Mode No.	Mode ETABS	Period (s)	UX	UY	UZ	Sum UX	Sum UY	Sum UZ	Sum RX	Sum RY	Sum RZ
1st	20	0.190	0.39	0.00	0	0.39	0.41	0	0.79	0.77	0.73
2nd	129	0.007	0.00	0.31	0	0.71	0.93	0	0.98	0.89	0.85
3rd	140	0.006	0.02	0.01	0	0.91	0.96	0	0.98	0.97	0.95

Table 4. The 7 SGM parameters from the PEER ground motion database.

S	RSN	EQ Name	Year	M_W	$\overrightarrow{V_{S30}}$ (m/s)	Mechanism	5–95% Duration (s)
S_1	1322	"Chi-Chi_ Taiwan"	1999	7.62	671	Reverse Oblique	27.90
S_2	1371	"Chi-Chi_ Taiwan"	1999	7.62	806	Reverse Oblique	38.20
S_3	1428	"Chi-Chi_ Taiwan"	1999	7.62	671	Reverse Oblique	22.70
S_4	1432	"Chi-Chi_ Taiwan"	1999	7.62	817	Reverse Oblique	28.70
S_5	1443	"Chi-Chi_ Taiwan"	1999	7.62	671	Reverse Oblique	24.60
S_6	1474	"Chi-Chi_ Taiwan"	1999	7.62	665	Reverse Oblique	18.10
S_7	1571	"Chi-Chi_ Taiwan"	1999	7.62	826	Reverse Oblique	36.20

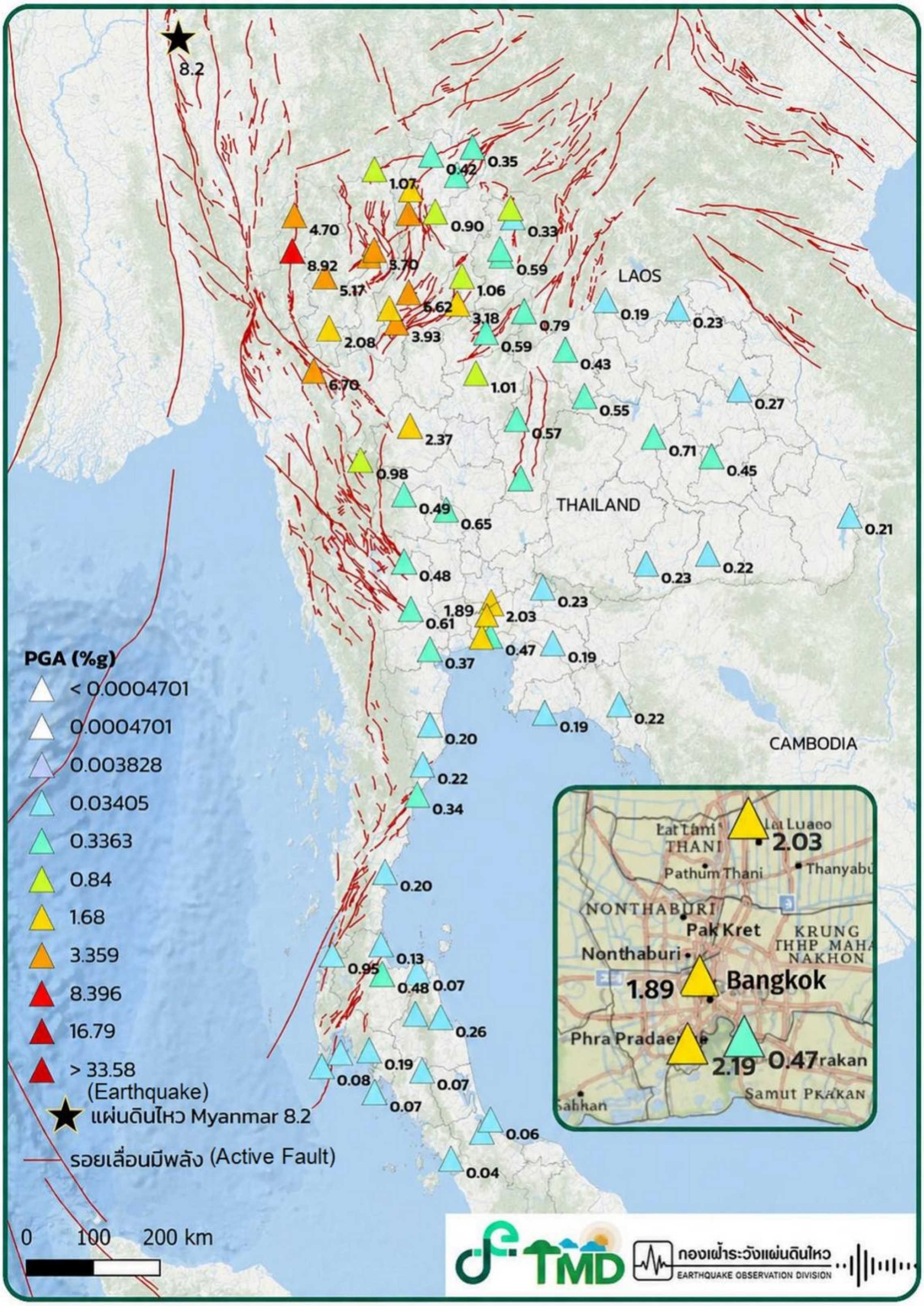

Figure 11. The ground acceleration (PGA) map from the magnitude 8.2 earthquake in Myanmar on March 28, 2025, at 13:20 local time, was recorded by EOD at TMD stations.

Source: The Earthquake Observation Division (EOD) under the Thai Meteorological Department (TMD).

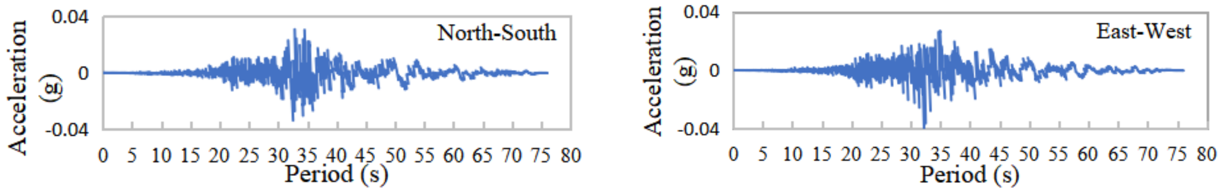

(**a**) S1-RSN 1322_ "Chi-Chi_ Taiwan".

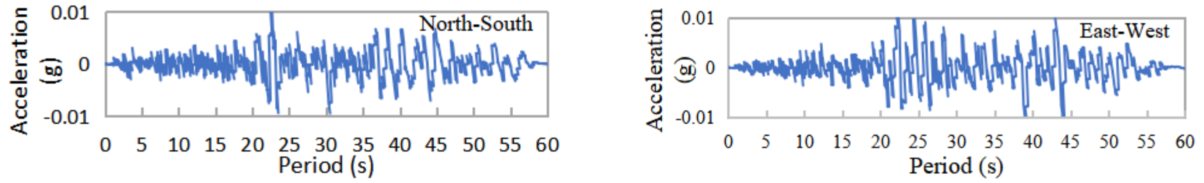

(**b**) S2-RSN1371_ "Chi-Chi_ Taiwan".

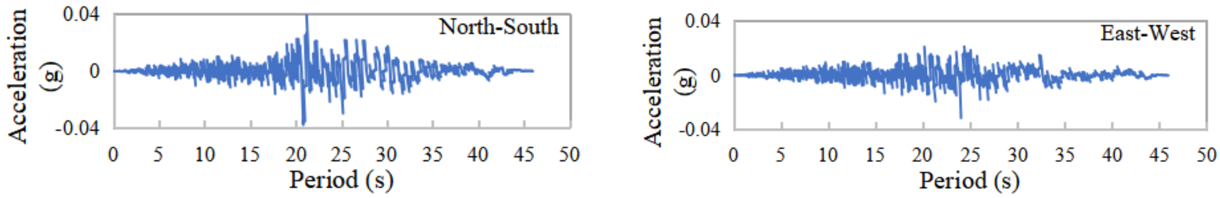

(**c**) S3-RSN1428_"Chi-Chi_ Taiwan".

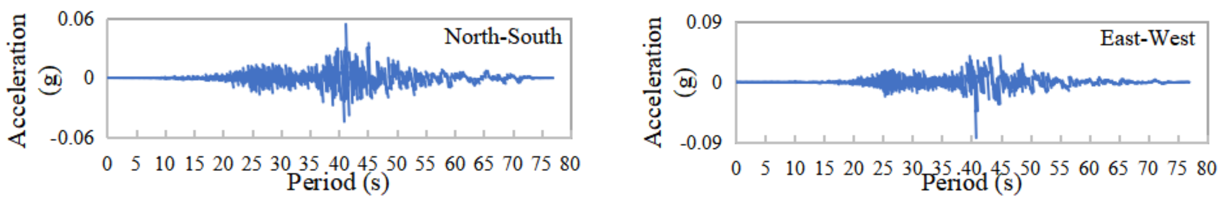

(**d**) S4-RSN1432_"Chi-Chi_ Taiwan".

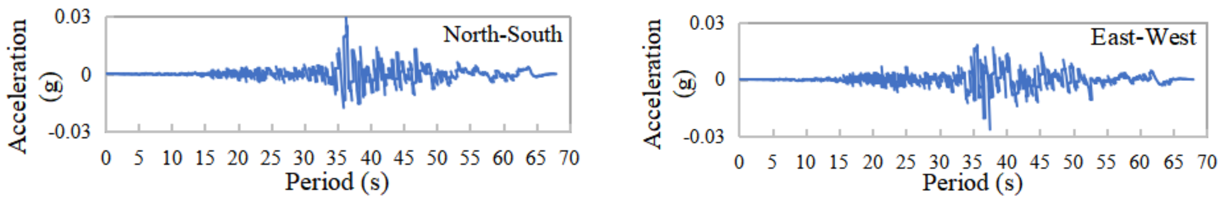

(**e**) S5-RSN 1443_"Chi-Chi_ Taiwan".

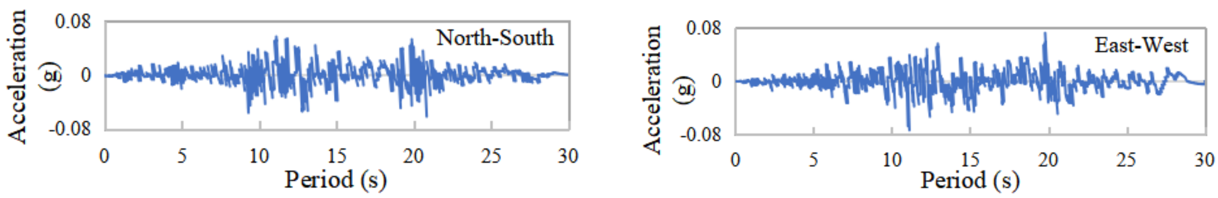

(**f**) S6-RSN1474_"Chi-Chi_ Taiwan".

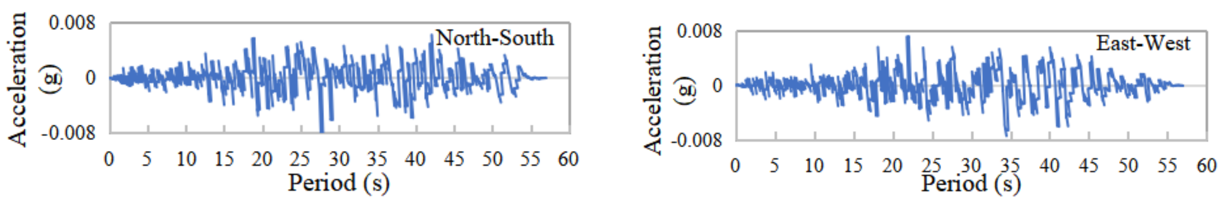

(**g**) S7-RSN1571_"Chi-Chi_ Taiwan".

Figure 12. Acceleration of the 7 SGMs in the north and east directions.

6.2.3. Spectral Matching

SeismoMatch's main function is to adjust ground-motion records so that their spectral acceleration response matches a target response spectrum. After loading some accelerograms and defining the target spectral response, the user needs only to define the matching algorithm, adjust the matching period range, set the required tolerance and press Do Matching. These parameters can either be defined on the main pre-processing window of the program or on the Matching parameters module of the Program Settings. Once the matching process is triggered, a pop-up window will be displayed showing the progress of each accelerogram as well as information on spectral misfit, iterations and tolerance. Several pieces of information are displayed for each matched accelerogram in this window, such as the matching outcome (converged or not), average misfit, maximum misfit, and number of iterations that were used. If convergence was not achieved for a given record, the user can always increase the number of iterations or the number of waves applied. In SeismoMatch, setting the scale factor to 1.0 means the input accelerogram's response spectrum is not pre-scaled before the matching process begins. It is used to match the raw motion (scaled to units like g or m/s^2) directly to the target spectrum, allowing the software to add wavelets to the original record's amplitude.

Figure 13 shows amplitude-scaled response spectra of the 7 SGMs for MCE-level UHS in the north and east directions. **Figure 14** shows spectral matching of the 7 SGMs for MCE-level UHS in the north and east directions.

6.2.4. Load Pattern

Table 5 shows the load (L) patterns: Item No.7: NLRHA1 to NLRHA7 are S1-RSN 1322, S2-RSN 1371, S3-RSN 1428, S4-RSN 1432, S5-RSN 1443, S6-RSN 1474, and S7-RSN 1571, respectively.

6.2.5. Load Combinations

Table 6 shows the load combinations according to ACI 318-99, ETABS [27] and AISC 360-22 [28].

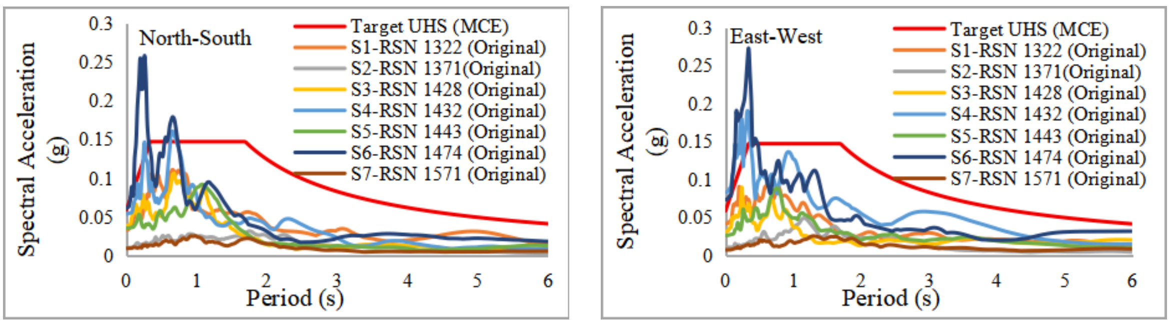

(**a**) North direction. (**b**) East direction.

Figure 13. Amplitude-scaled response spectra of the 7 SGMs for MCE-level UHS.

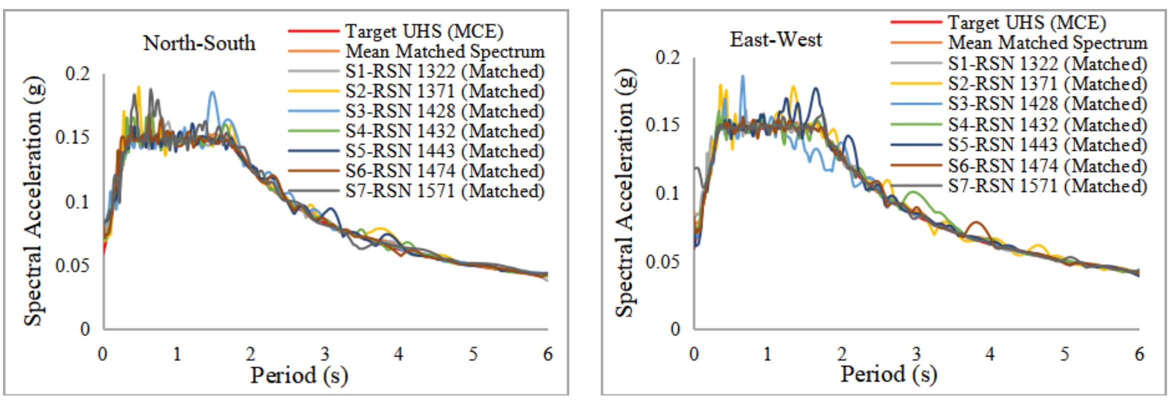

(**a**) North direction. (**b**) East direction.

Figure 14. Spectral matching, and the mean of the 7 SGMs for MCE-level UHS.

Table 5. Defined load patterns.

No.	Name	Type	Analysis Type	Auto Lateral Load	Self Weight Multiplier
1	DL	Static	Dead load	-	1
2	LL	Static	Reducible live load	-	0
3	SDL	Static	Superimposed dead load	-	0
4	WL	Static Dynamic	Wind load	ASCE 7-22	0
5	ELF, EQ	Static Dynamic	Equivalent static lateral force	ASCE 7-22	0
6	RS	Dynamic	Response spectrum	ASCE 7-22	0
7	NLRHA 1–7	Dynamic	Nonlinear response history	ASCE 7-22	0

Table 6. Load combinations.

Details of Load Combinations
1.40 DL + 1.40 SD
1.40 DL + 1.40 SD + 1.70 LL
1.05 DL + 1.05 SD + 1.275 LL ± 1.275 WLx
1.05 DL + 1.05 SD + 1.275 LL ± 1.275 WLy
0.90 DL + 0.90 SD ± 1.30 WLx
0.90 DL + 0.90 SD ± 1.30 WLy
1.05 DL + 1.05 SD + 1.275 LL ± 1.00 EQx
1.05 DL + 1.05 SD + 1.275 LL ± 1.00 EQy
0.90 DL + 0.90 SD ± 1.00 EQx
0.90 DL + 0.90 SD ±1.00 EQy
1.05 DL + 1.05 SD + 1.275 LL ± 1.00 RSx
1.05 DL + 1.05 SD + 1.275 LL ± 1.00 RSy
0.90 DL + 0.90 SD ± 1.00 RSx
0.90 DL + 0.90 SD ± 1.00 RSy

6.3. Structural Analysis and Design

The present structural analysis and design was applied using the loads in **Tables 5** and **6**, and was performed by SeismoMatch[29] and ETABS, so as to comply with ACI 318-99, AISC 341-22[30], AISC 358-22[31], AISC 360-22, ASCE 7-05, ASCE 7-22[32], ASCE 41-23[33], ASTM A36[34], ASTM A615, ASTM A500, ASTM A501, ASTM A572, ATC-40[35,36], BS EN 1991-1-4[37], DPT1301/1302-18, DPT 1302-09, DPT 1303-57[38], DPT 1304-18, DPT 1306-67[39], DPT 1311-07, EIT 1018-46[40], BS EN 1998-1: 2004[41], and 2021 IBC standards.

No effects of soil-structure interaction were considered. The described support conditions indicate that the bases of the 8 legs (**Figure 15**) are fully fixed against translation (UX, UY, UZ) and restricted in rotation (RX, RZ). Specifically, this setup represents a rigid, moment-resisting base connection, with one rotational direction (RY) released or released in some way to prevent localized over-constraint, potentially allowing for hinge-like behavior around that axis. Support Condition Summary: UX, UY, UZ (Fixed); the bases cannot move in the horizontal or vertical directions, RX, RZ (Fixed); the bases cannot rotate about the horizontal or vertical axes, and RY (Free); a rotational release, typically used in 3D modeling to prevent unintentional rigid behavior or to model pinned-like behavior in one direction. **Figure 16** shows the layout of nodes.

Figure 15. A survey revealing that the existing bases of the legs have no major deficiencies in alignment and leveling following the EQ indicates that the foundation system likely held its integrity.

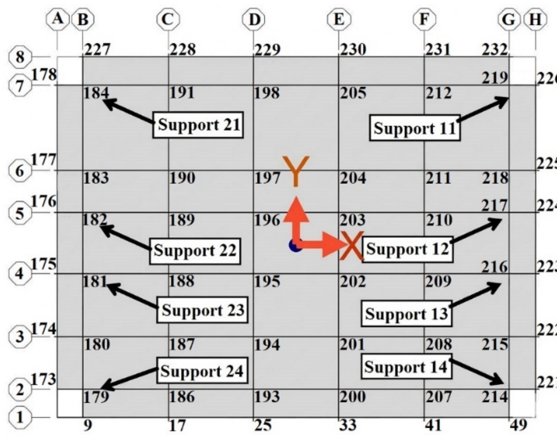

Figure 16. The layout of the nodes (Ns) of the applicable foundation loads (AFLs) for the eight column supports of the BKK observation wheel from the original structural analysis and design.

7. Results

Figure 17 shows the deformed shape and strength capacity of the structure which are both under the limits. **Table 7** shows DPT 1301/1302-18 standard limit, which is 0.02

(III), and **Table 8** shows ATC 40 IDR limit, which is 0.020 (PL-LS). **Figure 18a,b** shows the storey DPM comparison (x-axis and y-axis, respectively) of the NLRHA Nos. 1–7 with the average NLRHA (A-NLRHA). **Figure 18c,d** shows the storey DPM comparison (x-axis and y-axis, respectively) of the WL, ELF, RS and A-NLRHA with the DPM limit (H/90 = a height of the top of a wheel/90 = 53,250/90 = 600 mm) of the 2021 IBC. **Figure 19a,b** shows the IDR comparison (x-axis and y-axis, respectively) of the NLRHA Nos. 1–7 with A-NLRHA. **Figure 19c,d** shows the IDR comparison (x-axis and y-axis, respectively) of the WL, ELF, RS, and A-NLRHA with the IDR limit (0.020) of DPT 1301/1302-18, and ATC 40 standards. **Figure 20** shows that the max DPMs (x-axis and y-axis, respectively) of all loads, especially the WL are under the 2021 IBC DPM limit (600 mm). **Figure 21** shows that the max IDRs (x-axis and y-axis, respectively) of all loads are under the DPT 1301/1302-18 standard and the ATC 40 standard IDR limit (0.020). A-NLRHA is the average of NLRHA Nos. 1–7 as an Equation (1) shown below:

$$A - NLRHA = \frac{NLRHA_1 + NLRHA_2 + NLRHA_3 + NLRHA_4 + NLRHA_5 + NLRHA_6 + NLRHA_7}{7} \quad (1)$$

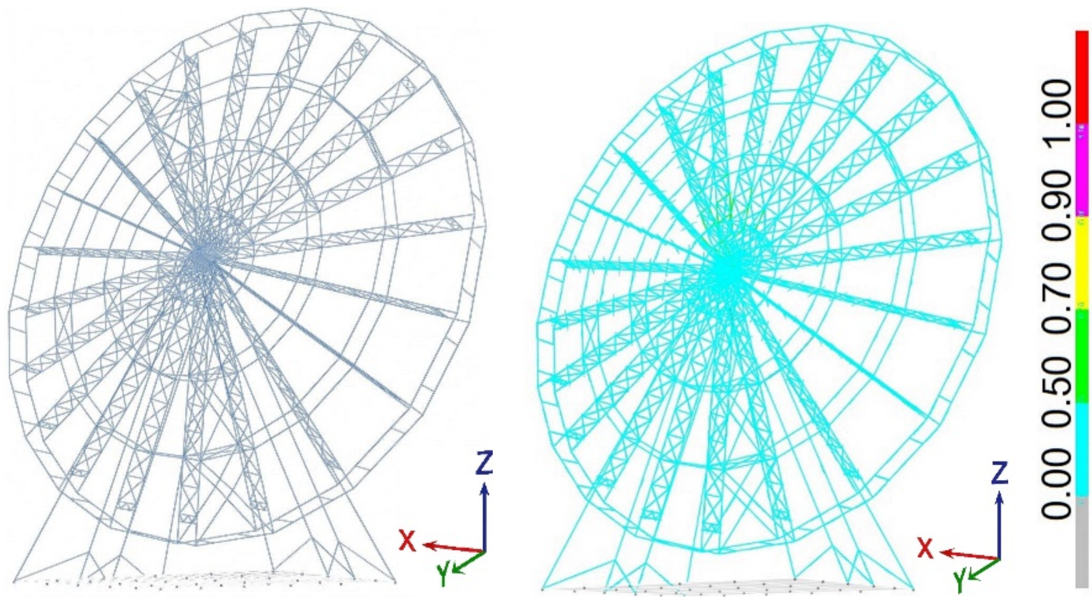

(**a**) (**b**)

Figure 17. (**a**) The structural analysis result: The deformed shape, and (**b**) the structural design result: The strength capacity.

Table 7. IDR limit: DPT 1301/1302-18 limit derived from ASCE 7-05 limit.

Structure	I or II	III	IV
Structures, other than masonry shear wall structures, four storeys or less above the base with interior walls, partitions, ceilings, and exterior wall systems that have been designed to accommodate the story drifts.	0.025	0.020	0.015
Masonry cantilever shear wall structures	0.010	0.010	0.010
Other masonry shear wall structures	0.007	0.007	0.007
All other structures	0.020	0.015	0.010

Table 8. IDR limit: ATC 40 standard limit.

IDR Limit	PL-IO	PL-DC	PL-LS	PL-SS
Max total IDR	0.010	0.010–0.020	0.020	$0.33V_i/P_i$, where V_i is the total calculated lateral shear force in storey i and P_i is the total gravity load at storey i.
Max total inelastic IDR	0.005	0.005–0.015	No limit	No limit

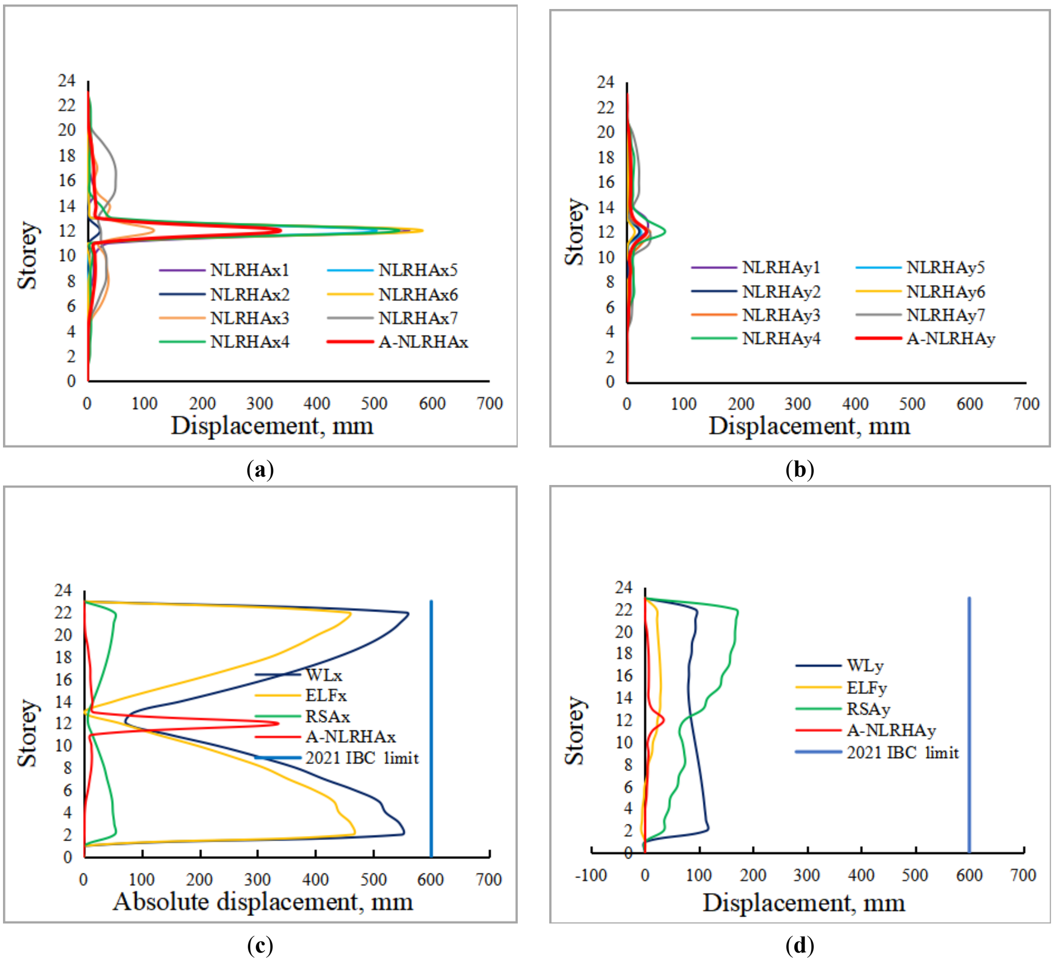

Figure 18. (**a**) The storey DPM comparison of the NLRHAx Nos. 1–7 and A-NLRHAx, (**b**) the storey DPM comparison of the NLRHAy Nos. 1–7, and A-NLRHAy, (**c**) the storey DPM comparison of the WLx, ELFx, RSAx, and A-NLRHAx with the 2021 IBC limit (600 mm), and (**d**) the storey DPM comparison of the WLy, ELFy, RSAy, and A-NLRHAy with the 2021 IBC limit (600 mm).

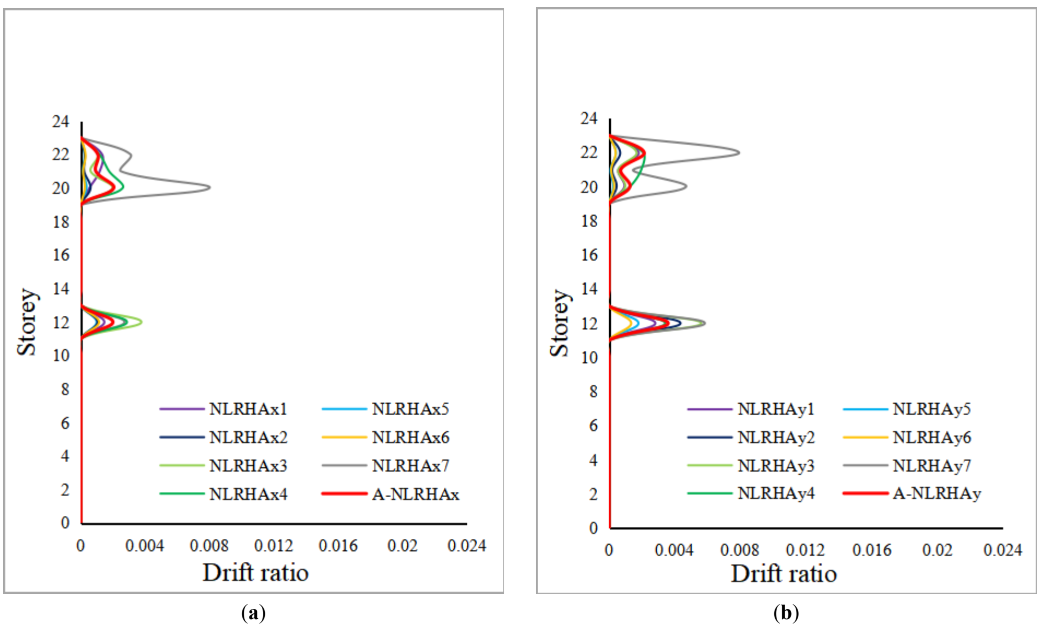

Figure 19. *Cont.*

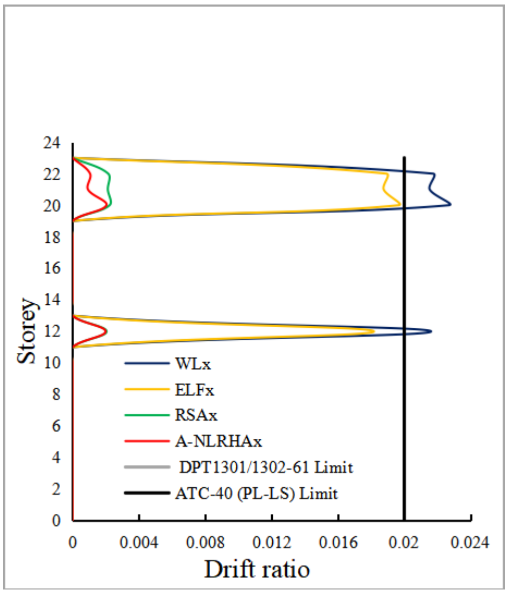

(c)

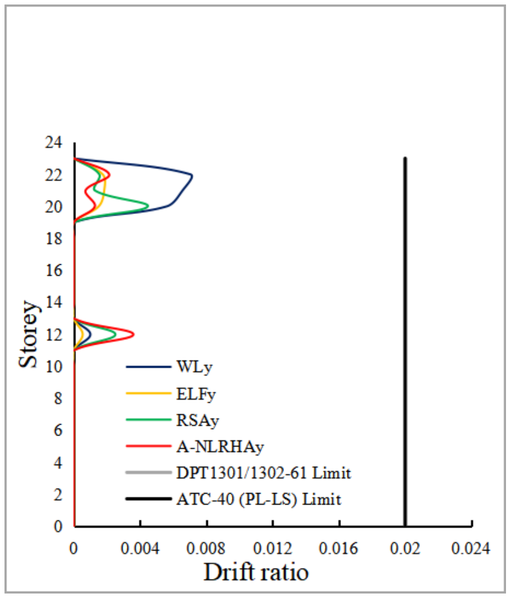

(d)

Figure 19. (**a**) The IDR comparison of the NLRHAx Nos. 1–7, and A-NLRHAx, (**b**) the IDR comparison of the NLRHAy Nos. 1–7, and A-NLRHAy, (**c**) the IDR comparison of the WLx, ELFx, RSAx, and A-NLRHAx with the ATC 40 (PL-LS), and DPT 1301/1302-18 limit (0.020) and (**d**) the IDR comparison of the WLy, ELFy, RSAy, and A-NLRHAy with the ATC 40 (PL-LS), and DPT 1301/1302-18 limit (0.020).

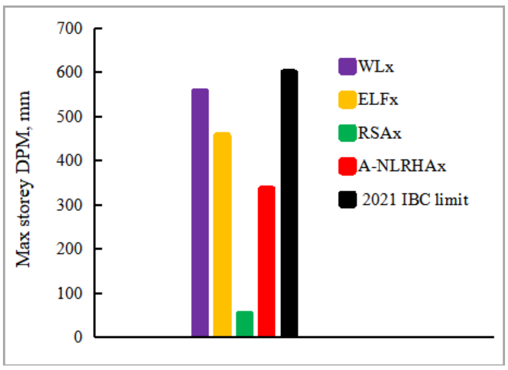

(**a**) Comparison of max storey DPM from the different load inputs with the 2021 IBC limit in x-axis.

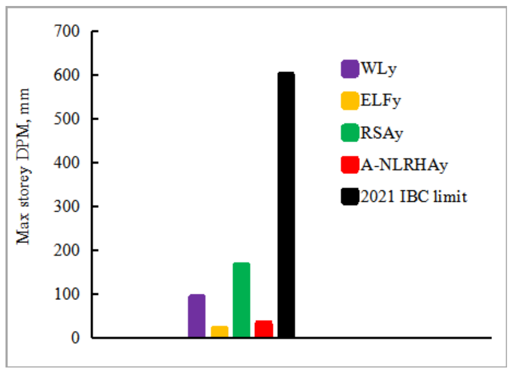

(**b**) Comparison of max storey DPM from the different load inputs with the 2021 IBC limit on the y-axis.

Figure 20. Comparison of max storey DPM from the different load inputs with the IBC 2021 limit.

Note: The 2021 IBC code, the DPM limit is 600 mm.

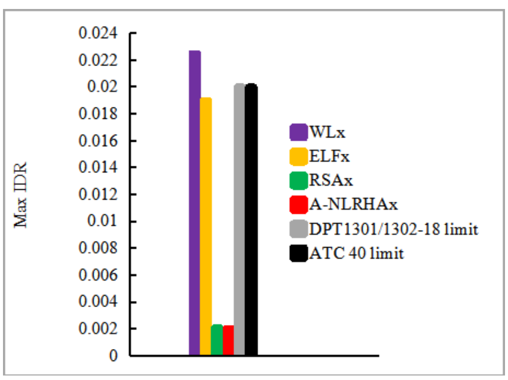

(**a**) Comparison of max IDRs from the different load inputs with the DPT1301/1302-18 and ATC 40 limits in x-axis.

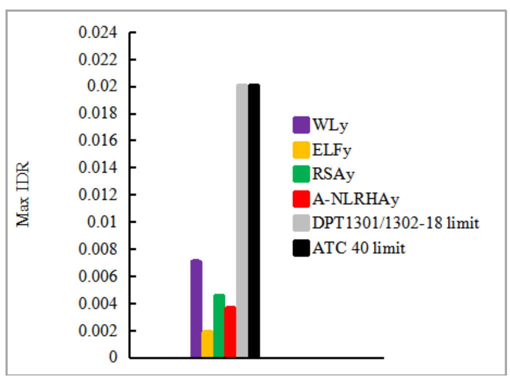

(**b**) Comparison of max IDRs from the different load inputs with the DPT1301/1302-18 and ATC 40 limits in the y-axis.

Figure 21. Comparison of max IDRs from the different load inputs with the DPT1301/1302-18 and ATC 40 limits.

Note: DPT1301/1302-18 and ATC 40 standard, the IDR limits are 0.020.

Based on structural analysis principles, if the wind load design results in **Table 9** are similar to the initial results in **Table 10**, it implies that the boundary conditions, wind speed parameters, and structural model applied to the present analysis were identical to the initial design input. The wind pressures, velocity pressure, and structural geometry are consistent between the two scenarios. Similar outputs suggest that the simulation model in **Table 9** successfully reproduced the structural response of the original analysis, serving as validation that the input loads were likely the same. **Table 11** shows the comparison of the applicable selected main member (**Figure 6a**) loads from the WL, ELF, RSA, and NLRHA (NL) Nos. 1–7, and A-NLRHA (A-NL).

Derived from the data presented in **Figures 20** and **21** and **Tables 9–12**, WL generates the maximum structural responses, including DPM, IDR, FZ, and P. These wind-induced responses exceed the results generated by seismic design parameters from the DPT 1301/1302-61 standard and the 7 selected ground motions, which were calculated using ELF, RSA, and A-NLRHA. Therefore, the foundation (F6) design is governed by WL rather than seismic shaking effects.

Table 9. The present AFLs from the structural analysis and design of this case study.

N	L	X-Axis						Y-Axis					
		FX (kN)	FY (kN)	FZ (kN)	MX (kN-m)	MY (kN-m)	MZ (kN-m)	FX (kN)	FY (kN)	FZ (kN)	MX (kN-m)	MY (kN-m)	MZ (kN-m)
11	DL	−106	61	321	65.5	0	7.1	−106	61.3	321	65.5	0	7.1
	LL	−13	8	49	2.1	0	−1.9	−13	8.2	49	2.1	0	−1.9
	W[1]	−136	70	284	−5.3	0	20	−136	−342	−1058	234	0	107
	W[2]	−31	−15	−63	2	0	7	−108	−73	−254	60	0	−27
	ELF	−20	14	52	2.8	0	−11	−20	−37	−131	16.0	0	7.4
	RSA	9.6	6	23	1.6	0	1.0	9.6	18.4	73	5.7	0	2.2
	A	16.1	6	33	33.6	0	13	16.1	6.9	43	31.2	0	11.2
12	DL	−114	−1	360	−8.1	0	−9.8	−114	−1.3	361	−8.1	0	−9.8
	LL	−15	−2	73	−0.4	0	−2.6	−15	−1.5	73	−0.4	0	−2.6
	W[1]	−149	1	309	−14	0	6.5	−149	−55	677	1436	0	69.7
	W[2]	−34	0	−69	4	0	2	81	−10	191	62	0	−29
	ELF	−22	0	55	0.0	0	0.5	−22	−2.7	58	9.7	0	4.8
	RSA	10.5	0	24	1.6	0	0.9	10.5	2.2	83	1.7	0	0.8
	A	18.4	2	43	25	0	20	18.4	1.6	51	22.9	0	16.0
13	DL	−115	1	363	8.6	0	9.9	−115	1.3	364	8.6	0	9.9
	LL	−15	2	73	0.6	0	2.6	−15	1.5	73.3	0.6	0	2.6
	W[1]	−149	−1	311	14.3	0	−6.6	−149	23.5	−663	109	0	55.5
	W[2]	−34	0	−69	−4	0	−2	−81	−10	−191	62	0	−29
	ELF	−22	−0	55	0.1	0	−0.5	−22	3.1	−57	7.1	0	3.7
	RSA	10.4	0.3	25	1.5	0	0.9	10.4	1.6	83	1.7	0	0.8
	A	14.2	7	50	20	0	19	14.2	5.4	36	16.2	0	16.7
14	DL	−106	−61	321	−65	0	−7.1	−106	−61	321	−66	0	−7.1
	LL	−13	−8	49	−2.1	0	1.9	−13	−8.2	49	−2.1	0	1.9
	W[1]	−136	−70	285	5.2	0	−20	−136	−295	1048	2346	0	108
	W[2]	−31	15	−63	−2	0	−7	108	−73	254	60	0	−27
	ELF	−20	−14	52	−2.9	0	11	−20	−33	130	16	0	7.4
	RSA	9.3	5.6	22	1.5	0	1.0	9.3	18.4	73	5.7	0	2.1
	A	11.9	6.1	38	29.4	0	13	11.9	7.8	36.5	24.3	0	11.8

Note: W[1] = 100 mph (1140 N/m^2) as per the design criteria and G_f = 2.35 for opened or special structures. W[2] = 85 mph as per the DPT 1311-07 standard and G_f = 0.85 for rigid structures.

Table 10. The original AFLs for the observation wheel from the original analysis.

N	L	X-Axis						Y-Axis					
		FX (kN)	FY (kN)	FZ (kN)	MX (kN-m)	MY (kN-m)	MZ (kN-m)	FX (kN)	FY (kN)	FZ (kN)	MX (kN-m)	MY (kN-m)	MZ (kN-m)
11	DL	−107	64.8	295	−68	0	14.7	−107	64.8	295	−68	0	14.7
	LL	−14	8.7	32.1	−0.1	0	−0.1	−14	8.7	32.1	−0.1	0	−0.1
	W[1]	−25	13.3	49.2	−0.4	0	−4.3	77	−59	−178	−28	0	−12
	WW[2]	−114	60.6	224	−1.8	0	−19	350	−268	−815	−13	0	−55

Table 10. *Cont.*

N	L	X-Axis						Y-Axis					
		FX (kN)	FY (kN)	FZ (kN)	MX (kN-m)	MY (kN-m)	MZ (kN-m)	FX (kN)	FY (kN)	FZ (kN)	MX (kN-m)	MY (kN-m)	MZ (kN-m)
12	DL	−117	−4	318	−12	0	−1	−117	−4	318	−12	0	−1
	LL	−15	−1.3	35.2	−1.4	0	−0.6	−15	−1.3	35.2	−1.4	0	−0.6
	W [1]	−27	−2.9	53.9	−1.9	0	−2.1	−79	−4.1	187	−18	0	−8.0
	WW [2]	−123	−13	245	−8.7	0	−9.6	−360	−18	853	−86	0.0	−36
13	DL	−117	4.0	318	12.6	0	−1.0	−117	4.0	318	12.6	0	−1.0
	LL	−15	1.3	35.2	1.4	0	0.6	−15	1.3	35.2	1.4	0	0.6
	W [1]	−27	2.9	53.9	1.9	0	2.1	78	−1.3	−186	−18	0	−7.8
	WW [2]	−123	13.1	245	8.7	0	9.6	358	−6.3	−848	−84	0	−35
14	DL	−107	−65	296	68	0	14.7	−107	−65	296	68	0	14.7
	LL	−13	−8.7	32	0.1	0	0.1	−13	−8.7	32	0.1	0	0.1
	W [1]	−25	−13	49	0.1	0	4.3	−76	−54	177	−28	0	−12
	WW [2]	−115	−61	224	1.8	0	19.6	−347	−246	810	−129	0	19.6
21	DL	107	64.8	296	−68	0	14.7	−107	64.8	296	−68	0	14.7
	LL	−14	8.7	32.1	−0.1	0	0.1	−14	8.7	32.1	−0.1	0	0.1
	W [1]	−25	−13	−49	0.6	0	−3.7	−77	−59	−180	−28	0	12
	WW [2]	−113	−61	−224	2.8	0	−17	−353	−269	821	−129	0	−17
22	DL	117	−4	318	−12	0	−1	117	−4	318	−12	0	−1
	LL	15	−1.3	35.2	−1.4	0	0.6	15	−1.3	35.2	−1.4	0	0.6
	W [1]	−27	4.3	−53	1.9	0	−2.1	79	−4.1	185	−18	0	8.0
	WW [2]	−122	19	−245	8.6	0	−9.1	362	−18	843	−86	0.0	−9.1
23	DL	117	4.0	318	12.6	0	1.0	117	4.0	318	12.6	0	1.0
	LL	15	1.3	35.1	1.4	0	−0.1	15	1.3	35.1	1.4	0	−0.1
	W [1]	−26	−4.3	−54	−1.9	0	2.0	−26	−4.3	−54	−1.9	0	2.0
	WW [2]	−122	−19	−245	−8.6	0	9.1	−360	−6.3	838	−83	0	35.9
24	DL	107	−65	296	68	0	−15	107	−65	296	68	0	−15
	LL	13.8	−8.7	32.1	0.1	0	−0.1	13.8	−8.7	32.1	0.1	0	−0.1
	W [1]	−25	13.5	−49	−0.1	0	3.7	76.8	−54	179	−28	0	12.0
	WW [2]	−113	61.7	−224	−2.9	0	16.9	350	−248	816	−129	0	54.9

Note: W [1]: Wind in Service, 250 N/m^2;WW [2]: Wind out of Service, 1140 N/m^2.

Table 11. Comparison of the applicable selected main member loads from the WL, ELF, RSA, and NLRHA Nos. 1–7, and A-NLRHA.

L	X-Axis						Y-Axis					
	P	V2	V3	T	M2	M3	P	V2	V3	T	M2	M3
	(kN)	(kN)	(kN)	(kN-m)	(kN-m)	(kN-m)	(kN)	(kN)	(kN)	(kN-m)	(kN-m)	(kN-m)
WL	224	0.01	0.77	0.28	0.12	0.03	−224	−0.0	0.7	−0.2	−0.10	−0.0
ELF	16	4.3	0.04	0.01	0.04	17.2	−55	−0.0	−0.1	−0.2	−0.00	−0.0
RSA	3	0.2	0.04	0.01	0.04	0.78	−7	−0.0	−0.7	−0.3	−0.42	−0.1
NL1	123	0.9	5.77	0.28	3.70	0.20	−123	−0.1	−5.2	−0.3	−9.55	−0.6
NL2	27	0.1	1.03	0.61	1.21	0.34	−33	−0.9	−0.7	−0.4	−1.05	−2.3
NL3	31	0.6	1.07	0.55	1.52	0.68	−21	−0.1	−1.0	−0.2	−1.30	−0.4
NL4	239	0.1	9.80	0.52	17.9	0.36	−234	−2.2	−10	−1.6	−18.7	−8.2
NL5	166	0.4	1.71	0.30	2.08	0.18	−113	−0.4	−2.4	−0.4	−2.96	−0.5
NL6	148	0.4	2.92	0.43	3.56	0.28	−233	−0.4	−2.2	−0.5	−2.84	−0.6
NL7	37	0.6	0.89	0.38	1.27	0.68	−37	−0.3	−1.0	−0.4	−1.22	−0.8
A−NL	111	0.4	3.31	0.44	4.47	0.39	−114	−0.6	−3.3	−0.6	−5.39	−1.9

Table 12. The summary of the max results (DPM, IDR, FZ, and P) of WL, ELF, RSA, and A-NLRHA.

L	DPM (mm)	IDR (Ratio)	FZ (kN)	P (kN)
WL	557	0.0225	W [1] = 1058.5 and W [2] = 258	224
ELF	458	0.0190	130.8	55
RSA	167	0.0045	83.4	7
A-NLRHA	210	0.0020	50.7	114

Figure 22 shows the layout of the foundation F6. The F6 was designed by using the max results of AFLs in order to be able to use F6 for supporting every leg column in case of a change in the direction of loads. **Figure 23** shows the minimum rebar areas in F6 on the x-axis of 108 cm^2 and the y-axis of 65 cm^2, which are more than the required rebar areas from the original design on the x-axis of 13 cm^2 and the y-axis of 15 cm^2, and the present design on the x-axis of 16 cm^2 and the y-axis of 18 cm^2. The original max total design loads of F6 are 1,270 kN for compression and −30 kN for tension, and the present max total design loads of F6 are 1,406 kN for compression and −201 kN for tension. F6 is supported by 6-piles (allowable compression load is 200 kN per pile for a safety factor of 2.5, and allowable tension load is −70 kN per pile). Thus, new max design loads on each pile = 1406/6 = 23.50 kN (compression) for a safety factor of 2.10, and −201/6 = −33.5 kN (tension) which is less than −70.0 kN per pile, which are both acceptable.

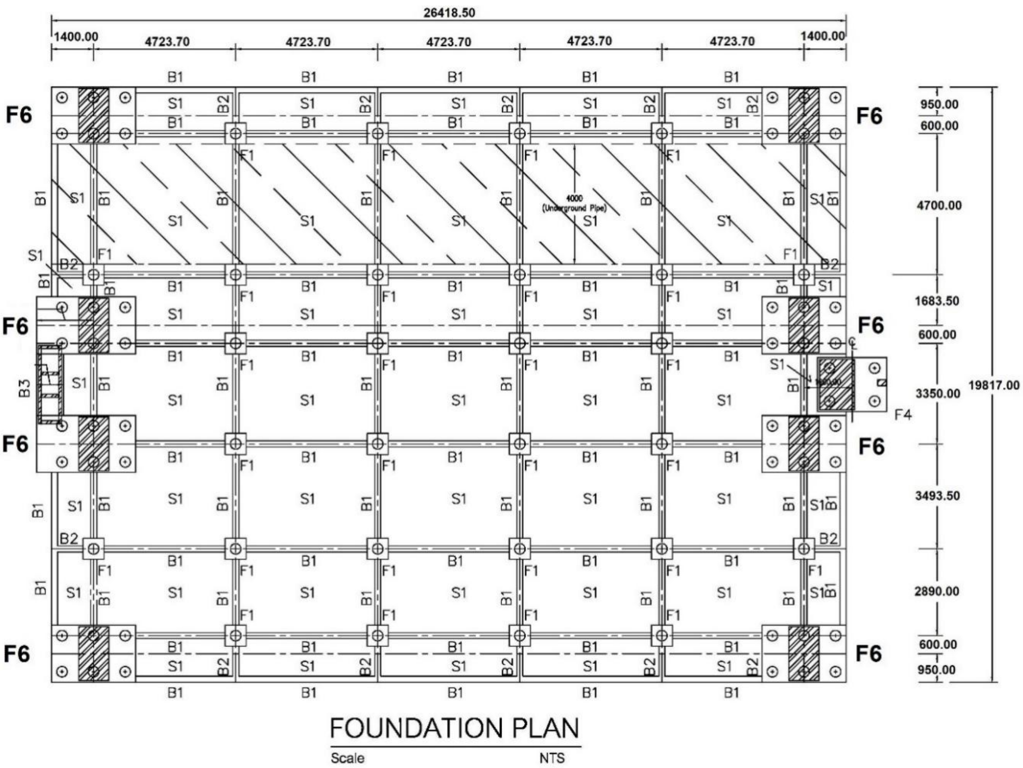

Figure 22. Ground floor framing plan and the layout of the foundations No. 6 (F6).

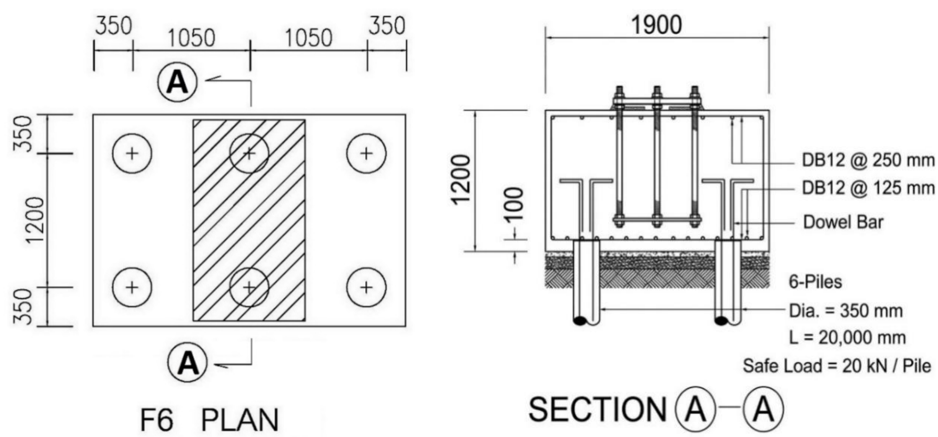

(**a**) (**b**)

Figure 23. (**a**) The F6 plan with 6-bored piles and (**b**) the section A–A.

8. Discussions

Effective parameters for EQ forces for structures defined by codes are zone factors according to their locations, importance factors of structures, and kinds of structural systems. Effective parameters for WLs affecting structures are areas subjected to wind as well as intensities of wind pressures defined by codes according to their locations, and kinds of structural systems.

As the height of a structure increases, WLs generally become more dominant than EQ loads, as wind pressure increases significantly with altitude due to less friction, whereas lower-rise buildings are often more vulnerable to seismic forces. Tall buildings are more flexible and have longer natural vibration periods, often reducing the base shear caused by EQs but increasing susceptibility to wind-induced vibrations.

Prior to this new understanding, the code-prescribed design-basis EQ loading was considered lower than the WLs. Therefore, most of the existing high-rise buildings in BKK were primarily designed for WLs without considering significant seismic action and ductile detailing requirements.

For this case study, the WL parameters are very high values, such as the wind speed design, "wind out of service", is 100 mph (1,140 N/m²), and the gust factor (G_f) is 2.35 for opened or special structures, indicating intense dynamic amplification of WLs, significantly exceeding typical rigid structure values (~0.85). This high value signifies that turbulence and wind gusts are causing substantial fluctuating responses, requiring careful consideration of structural damping, stiffness, and potential resonance effects, often requiring dynamic analysis. While the seismic parameters of zone 5 (damping = 2.5%) are low values, such as the parameters of the case study for MCE, 2% in 50 years at 0.2 s for S_{DS} dynamic is 0.148 g, and at 1.0 s for S_{D1} dynamic is 0.25 g. Notwithstanding, even for cases where the wind demands determine the design of the lateral load-resisting system, a detailed performance-based seismic evaluation should be carried out to ensure overall structural safety and integrity.

9. Conclusions

This study presents the resilience of the existing observation wheel steel structure for resisting the seismic loads of an EQ, in particular the 28 March 2025 Mw 7.7 Mandalay EQ. The study provides a structural analysis and design stepwise example starting with the 3-D model proposed by using ETABS, and adjusting ground-motion records so that their spectral acceleration response matches a target response spectrum by using SeismoMatch. The following conclusions can be drawn:

(1) From **Table 12**, the max DPMs of 557 mm for WL, 458 mm for ELF, 167 mm for RS, and 210 mm for A-NLRHA are under the IBC 2021 code, DPM limit of 600 mm.

(2) From **Table 12**, the max IDRs of 0.0190 for ELF, 0.0045 for RS, and 0.0020 for A-NLRHA under the ATC, and DPT 1301/1302-61 standards, with an IDR limit of 0.020.

(3) From **Table 12**, the max vertical loads (FZs) of 130.8 kN for ELF, 83.4 kN for RS, and 50.7 kN for A-NLRHA on the foundation (F6) are less than the max vertical loads (FZs) of 1058.5 kN for WL1 and 258 kN for WL2 on the foundation (F6). As a result, the shaking effects from the EQ on the foundations are less than the forces from the wind. Thus, the wind governed the foundation design of the existing structure.

(4) From **Table 12**, the max axial loads (Ps) of 55 kN for ELF, 7 kN for RS, and 114 kN for A-NLRHA are less than the max axial load (P) of 224 kN for WL. As a result, the shaking effects from the EQ in the existing steel main member are less than the forces from the wind. Thus, the wind governed the steel design of the existing steel main structure as well.

(5) Consequently, the observation wheel has adequate resilience for resisting seismic loads from EQs, as shown by the March 28, 2025 Mw 7.7 Mandalay EQ.

(6) Therefore, even for cases where the wind demands determine the design of the lateral load-resisting system, a detailed performance-based seismic evaluation should be carried out to ensure overall structural safety and integrity.

Funding

This work received no external funding.

Institutional Review Board Statement

This study did not involve human participants, clinical trials, or the collection of sensitive personal data. Therefore, an Institutional Review Board (IRB) approval was not required.

Informed Consent Statement

Informed consent was obtained from participants, and confidentiality was maintained throughout the study.

Data Availability Statement

The data that support the findings of this study are available within the article.

Conflicts of Interest

The author declares that there is no conflict of interest.

References

[1] Ornthammarath, T., Warnitchai, P., Maruyama, Y., et al., 2025. Far-Field Ground Motion Characteristics of the Bangkok Basin, Thailand, in the 2025 Mw 7.7 Mandalay Earthquake: Initial Insights. Bulletin of Earthquake Engineering. 23, 6577–6602.

[2] United States Geological Survey (USGS), 2025. M7.7 – 2025 Mandalay, Burma (Myanmar) Earthquake. Available from: https://earthquake.usgs.gov/earthquakes/eventpage/us7000pn9s/executive (cited 10 May 2025).

[3] Thilakarathna, N.S., Anwar, N., Norachan, P., et al., 2018. The Effect of Wind Loads on the Seismic Performance of Tall Buildings. Athens Journal of Technology and Engineering. 5(3), 251–276. DOI: https://doi.org/10.30958/ajte.5-3-3

[4] Thilakarathna, N.S., Anwar, N., 2021. Seismic Performance Evaluation of a Wind Governed Concrete Tall Building. In Proceedings of the 115th Annual Session of the Institute of Engineers Sri Lanka, Online, 6 August 2021; pp. 1–10.

[5] Thilakarathna, S.N., Fernando, S., Anwar, N., 2020. The Effect of Wind Loads on the Seismic Performance of Tall Buildings in Sri Lanka and Thailand. Society of Structural Engineers Sri Lanka: Colombo, Sri Lanka.

[6] Pillai, B., Guha, P., 2015. Comparison between RCC and Steel Structure with Wind and Earthquake Effect using STAAD Pro. International Journal of Applied Research. 1(6), 28–33.

[7] Ministry of Interior, 1997. Ministerial Regulation No.49, B.E. 2540 (1997) Issued pursuant to the Building Control Act, B.E. 2522 (1979). Ministry of Interior: Bangkok, Thailand. Available from: https://lkbie.go.th/handbook/Program_IEAT/pages/en/Department/MOI.html# (in Thai)

[8] DPT 1302-52 Standard. 2009. Standard for Earthquake Resistant Design of Buildings. Department of Public Works and Town & Country Planning, Ministry of Interior: Bangkok, Thailand. (in Thai)

[9] United States Geological Survey (USGS), 2014. M6.1 – 32 km South Southwest (SSW) of Chiang Rai, Thailand. Earthquake Hazards Program. Available from: https://earthquake.usgs.gov/earthquakes/eventpage/usb000qack/executive (cited 10 May 2025).

[10] Poovarodom, N., Jirasakjamroonsri, A., Warnitchai, P., 2017. Development of New Design Spectral Accelerations for Bangkok Considering Deep Basin Effects. In Proceedings of the 16th World Conference on Earthquake Engineering, Santiago, Chile, 9–13 January 2017.

[11] DPT 1301/1302-61 Standard. 2018. Standard for Earthquake Resistant Design of Buildings. Department of Public Works and Town & Country Planning, Ministry of Interior: Bangkok, Thailand. (in Thai)

[12] Poovarodom, N., Warnitchai, P., Ornthammarath, T., et al., 2018. A New Earthquake Resistant Design Standard for Buildings in Thailand. In Proceedings of the 7th Asia Conference on Earthquake Engineering, Bangkok, Thailand, 22–25 November 2018. Available from: https://dspace.spu.ac.th/handle/123456789/5894

[13] Buddee, S., 2016. Giant Observation Wheel in Bangkok. In Proceedings of the IABSE Conference "Bridges and Structures Sustainability – Seeking Intelligent Solutions", Guangzhou, China, 8–11 May 2016.

[14] ACI 318-99. 1999. Building Code Requirements for Structural Concrete (ACI 318-99) and Commentary (ACI 318R-14). American Concrete Institute: Farmington Hills, MI, USA.

[15] Buddee, S., 2025. Prevention of Foundation Flood Damage Using Pile-Cap Connections. In Proceedings of the IABSE Symposium 2025: Environmentally Friendly Technologies and Structures – Focusing on Sustainable Approaches, Tokyo, Japan, 18–21 May 2025; pp. 1408–1416.

[16] ASTM A615. 2022. Standard Specification for Deformed and Plain Carbon-Steel Bars for Concrete Reinforcement. American Society for Testing and Materials: West Conshohocken, PA, USA.

[17] ASTM A500. 2017. Standard Specification for Cold-Formed Welded and Seamless Carbon Steel Structural Tubing in Rounds and Shapes. American Society for Testing and Materials: West Conshohocken, PA, USA.

[18] ASTM A501. 2021. Standard Specification for Hot-Formed Welded and Seamless Carbon Steel Structural Tubing. American Society for Testing and Materials:

West Conshohocken, PA, USA.
[19] ASTM A572. 2017. Standard Specification for High-Strength Low-Alloy Columbium-Vanadium Structural Steel. American Association State Highway and Transportation: Washington, DC, USA.
[20] DPT 1304-61 Standard. 2018. Seismic Resistance Design of Steel Buildings. Department of Public Works and Town & Country Planning, Ministry of Interior: Bangkok, Thailand. (in Thai)
[21] BS EN 12385. 2020. Steel Wire Ropes – Safety for Lifting Applications. British Standards Institution: London, UK.
[22] Boonyapinyoa, V., Poovarodoma, N., Limsamphancharoenb, N., et al., 2010. Wind Loading Standard for Building Design in Thailand and Country Report 2010. Available from: https://www.wind.arch.t-kougei.ac.jp/APECWW/Report/2010/Thailand.pdf (cited 10 May 2025).
[23] ASCE 7-05. 2005. Minimum Design Loads for Buildings and Other Structures. American Society of Civil Engineers: Reston, VA, USA.
[24] DPT 1311-50 Standard. 2007. Wind Loading Calculation and Response of Buildings. Department of Public Works and Town & Country Planning, Ministry of Interior: Bangkok, Thailand. (in Thai)
[25] 2021 IBC. 2021. Table 1604.3a: Deflection Limit. International Building Code. International Code Council: Country Club Hills, IL, USA.
[26] PEER, 2025. PEER Ground Motion Database. Available from: https://ngawest2.berkeley.edu (cited 7 May 2025).
[27] ETABS V.22.6.0. 2022. Structural and Earthquake Engineering Software: Building Analysis and Design. Computers and Structures, Inc.: Walnut Creek, California, USA.
[28] AISC 360-22. 2022. Specification for Structural Steel Buildings. American Institute of Steel Construction: Chicago, IL, USA.
[29] SeismoMatch Release-1. 2021. Earthquake Software for Response Spectrum Matching. Seismosoft: Pavia, Italy.
[30] AISC 341-22. 2022. Seismic Provisions for Structural Steel Buildings. American Institute of Steel Construction: Chicago, IL, USA.
[31] AISC 358-22. 2022. Prequalified Connections for Special and Intermediate Steel Moment Frames for Seismic Applications (ANSI/AISC 358-22). American Institute of Steel Construction: Chicago, IL, USA.
[32] ASCE 7-22. 2022. Minimum Design Loads for Buildings and Other Structures. American Society of Civil Engineers: Reston, VA, USA.
[33] ASCE/SEI 41-23. 2023. Seismic Evaluation and Retrofit of Existing Buildings. American Society of Civil Engineers: Reston, VA, USA.
[34] ASTM A36. 2019. Standard Specification for Carbon Structural Steel. American Society for Testing and Materials: West Conshohocken, PA, USA.
[35] ATC-40. 1996. Seismic Evaluation and Retrofit of Concrete Buildings. Applied Technology Council: Redwood City, CA, USA.
[36] Buddee, S., 2024. Comparative Analysis of ATC 40 and DPT 1301/1302-61 for Seismic Performance of Buildings using NLRHA. In Proceedings of the 18th World Conference on Earthquake Engineering, Milan, Italy, 30 June–5 July 2024.
[37] BS EN 1991-1-4. 2005. Actions on Structures–General Actions–Wind Actions. British Standards Institution: London, UK.
[38] DPT 1303-57 Standard. 2014. Seismic Assessment and Retrofitting Standards for Buildings in Earthquake-Prone Areas. Department of Public Works and Town & Country Planning, Ministry of Interior: Bangkok, Thailand. (in Thai)
[39] DPT 1306-67 Standard. 2024. Welding Connection Standards for Structural Steel Buildings for Earthquake Resistance. Department of Public Works and Town & Country Planning, Ministry of Interior: Bangkok, Thailand. (in Thai)
[40] EIT 1018-46 Standard. 2003. Wind Loading Code for Building Design, Table 2.2.1a: Deflection Limit. Engineering Institute of Thailand: Bangkok, Thailand. (in Thai)
[41] BS EN 1998-1-1. 2024. Eurocode 8: Design of Structures for Earthquake Resistance – Part 1: General Rules, Seismic Actions and Rules for Buildings. European Committee for Standardization: Brussels, Belgium.